Different Kinds of Tetrahedral V Species in Vanadium-Containing Zeolites Evidenced by Diffuse Reflectance UV-vis, Raman, and Periodic Density Functional Theory

ARTICLE *in* THE JOURNAL OF PHYSICAL CHEMISTRY C · NOVEMBER 2010

Impact Factor: 4.77 · DOI: 10.1021/jp107589d

Different Kinds of Tetrahedral V Species in Vanadium-Containing Zeolites Evidenced by Diffuse Reflectance UV−vis, Raman, and Periodic Density Functional Theory

Anna E. Lewandowska,*,† Miguel A. Banares,† Frederik Tielens,‡,§ Michel Che,‡,§,|| and Stanislaw Dzwigaj*,‡,§

Catalytic Spectroscopy Laboratory, Institute of Catalysis and Petroleum Chemistry, CSIC, E-28049-Madrid, Spain, Laboratoire de Réactivité de Surface, UPMC Univ Paris 6, 4 Place Jussieu, 75252 Paris Cedex 05, France, Laboratoire de Réactivité de Surface, CNRS, UMR 7197, 4 Place Jussieu, 75252 Paris Cedex 05, France, and Institut Universitaire de France, 103 Bd. Saint-Michel, 75005 Paris, France

Received: August 11, 2010; Revised Manuscript Received: October 14, 2010

The combined use of DR-UV−vis and Raman spectroscopies allows one to evidence three kinds of tetrahedral V^V with different structure in V_xSiBEA zeolite. In all cases, vanadium species possess distorted tetrahedral configuration. At very low vanadium content (0.05 wt %), the majority of tetrahedral V(V) species are strongly distorted and have a nonhydroxylated pyramidal structure $(SiO)_3V{=}O$ with V═O stretching at 1054 cm^{-1} whereas the remaining tetrahedral V(V) species are less distorted with a hydroxylated pyramidal structure $(SiO)_2(HO)V{=}O$ with V═O stretching at 1018 cm^{-1}. In contrast, at higher vanadium contents (0.2−2 wt %), the main distorted V(V) species possess a nonhydroxylated pyramidal structure $(SiO)_3V{=}O$ with V═O stretching at 1033−1036 cm^{-1}. Periodic density functional theory (DFT) calculations confirm the presence of at least two different types of V site in V-containing zeolites. The experimental Raman bands recorded for V_xSiBEA with low and high V content were confirmed on the basis of DFT calculations related to seven vanadium model sites. The difficulty to assign the vibrations in V-containing silica materials is due to the overlap of the different critical vibrational fingerprints (V═O, and Si−O−V vibration modes). Moreover, it was found that H-bond formation with a V═O group is not energetically favorable.

1. Introduction

In situ characterization of vanadium-containing silica-based materials by Fourier transform infrared (FT-IR), electron paramagnetic resonance (EPR), X-ray absorption spectroscopy (XAS), diffuse reflectance (DR) UV−visible, ^{51}V NMR, and photoluminescence[1−9] has allowed one to obtain precise information on the nature and local environment of vanadium, and the use of resonance effect has helped to clearly assign the Raman bands of supported vanadium oxide species in the 1100−800 cm^{-1} window.[46] In the case of V-silicalites it was shown,[1,2,4,8] that vanadium is present as isolated distorted tetrahedra with a terminal vanadyl group (V═O) and a structure different from that of isolated distorted tetrahedral VO_4 units in HMS[8] or on SiO_2.[2]

Recently,[5−7,9−11] the nature and environment of vanadium(V) ions incorporated in dealuminated BEA zeolite (V_xSiBEA) by a two-step postsynthesis method were characterized using various techniques.

Because of the absence of d−d transitions in the range 600−800 nm in the DR UV−vis spectra and V(IV) EPR signal, the DR UV−visible bands observed at 270 and 340 nm for V_xSiBEA were assigned to oxygen-to-tetrahedral V(V) charge transfer transitions involving oxygen in bridging (V−O−Si) and terminal (V═O) positions.[5−7,9] Similar bands were also observed for various V-loaded silica-based materials[13−18] and assigned to distorted tetrahedral V(V) with one double V═O bond and three single V−O bonds forming a pyramidal structure.[19,20]

The presence of distorted tetrahedral V(V) species in V_xSiBEA zeolites has been confirmed by ^{51}V magic-angle spinning (MAS) NMR studies, which reveal a peak at −633 ppm.[21] In contrast with V species grafted onto a SiO_2 surface or introduced in mesoporous siliceous materials,[16−18,22,23] it was shown that distorted tetrahedral V(V) species are stable in ambient moisture in V_xSiBEA zeolites, whereas on SiO_2 or mesoporous materials, vanadium changes spontaneously from tetrahedral to octahedral coordination. A particular environment of vanadium in the zeolite framework (vanadium with one V═O group linked by three V−OSi bonds to the zeolite walls) was suggested to be responsible for the higher tolerance to ambient moisture.[6] Density functional theory (DFT) calculations evidence the high hydrophobicity of the zeolitic V-sites.[12]

The use of a second derivative presentation[7,11,21] allowed one to distinguish three types of vibrational fine structure in V_xSiBEA zeolites,[24] corresponding to three types of distorted tetrahedral vanadium species. The energy separation between the (0→0) and (0→1) vibrational levels were measured to be 1018 cm^{-1} for the least distorted tetrahedral V(V) species with a pyramidal structure $(SiO)_2(HO)V{=}O$ interacting with two nearby HOSi groups, 1036 cm^{-1} for the tetrahedral V(V) species with a nonhydroxylated pyramidal structure $(SiO)_3V{=}O$ interacting with one nearby HOSi group, and 1054 cm^{-1} for the most distorted tetrahedral V(V) species with a nonhydroxylated pyramidal structure $(SiO)_3V{=}O$ without any interaction with HOSi group.

On the basis of these experimental data and DFT calculations,[12] it was concluded from the relative stability of the different VO_xH_y-sites, that the IR bands at 3650 and 3620 cm^{-1}

* To whom correspondence should be addressed. E-mail: (S.D.) stanislaw.dzwigaj@upmc.fr; (A.E.L.) anna_lewandowska@icp.csic.es.
† Institute of Catalysis and Petroleum Chemistry, CSIC.
‡ UPMC Univ Paris 6.
§ CNRS, UMR 7197.
|| Institut Universitaire de France.

10.1021/jp107589d
Published on Web 11/02/2010

are characteristic of a metastable pentacoordinated $(SiO)_4VOH$ site, distributed on two crystallographic sites of the BEA zeolite, and that $(SiO)_3V{=}O$ is the most stable tetrahedral site.[12]

This work presents a comparative investigation by FTIR, Raman, and diffuse reflectance UV−vis of V_xSiBEA, and by DFT calculations of vanadium in sodalite structure, related to different vanadium sites in V_xSiBEA. Nevertheless, it is not clear if these sites are originating from the crystal structure or from the chemical/molecular environment of the V site. So, this point will be also discussed.

2. Experimental Section

2.1. Material Preparation. The TEABEA sample with a framework Si/Al ratio of 11 was provided by RIPP (China). It was dealuminated by treatment by a 13 mol·L^{-1} HNO_3 solution for 4 h at 353 K according to the procedure described by Bourgeat-Lami et al.[25] The dealuminated SiBEA zeolite thus obtained (Si/Al > 1300) was recovered by centrifugation washed with distilled water and dried overnight at 353 K.

The SiBEA sample was contacted with an aqueous solution of ammonium metavanadate in great excess (2.3 g zeolite in 10 mL of NH_4VO_3 solution). Because of the low concentration (10^{-2} to 10^{-3} mol·L^{-1}) and pH = 2.5, the initial aqueous solution of NH_4VO_3 is expected to mainly contain monomeric VO_2^+ ions.[26−28] The concentration of NH_4VO_3 solution was varied from 0.25×10^{-2} to 7×10^{-2} mol·L^{-1}. The suspension was left for 3 days at room temperature without any stirring. The solids were recovered by centrifugation and dried in air at 353 K overnight. V_xSiBEA samples with low (0.05 V wt %) and high (0.2, 0.9, and 2.0 V wt %) V content were prepared and labeled $V_{0.05}$SiBEA, $V_{0.2}$SiBE, $V_{0.9}$SiBEA, and $V_{2.0}$SiBEA, respectively.

2.2. Characterization. The chemical analysis of samples was performed with inductively coupled plasma atom emission spectroscopy at the CNRS Centre of Chemical Analysis (Vernaison, France).

Diffuse reflectance UV−visible spectra were recorded at 298 K in the range of 200−800 nm on a Cary spectrometer 5E equipped with a reflectance attachment.

Raman spectra were run with a single-monochromator Renishaw System-1000 microscope Raman equipped with a cooled charge-coupled device detector (200 K) and holographic Edge filter. The powder samples were excited with the 514 nm Ar^+ line; spectral resolution was ca. 3 cm^{-1} and spectrum acquisition consisted of 30 accumulations of 30 s. The spectra were obtained under oxidative conditions in an in situ hot stage (Linkam TS-1500). To avoid the fluorescence, prior to Raman spectra acquisition, the zeolites samples were calcined in flowing air at 773 K for 2 h at a rate of 10 K·min^{-1} and then cooled to 423 K in flowing air. Raman spectra were recorded at 773 K after dehydration of the samples.

2.3. Computational Details. Calculations were performed using ab initio plane-wave pseudopotential calculations implemented in VASP.[29,30] The Perdew−Burke−Ernzerhof (PBE) functional[31−33] was chosen to perform the periodic DFT calculations with an accuracy on the overall convergence tested elsewhere.[34−37] The valence electrons were treated explicitly and their interactions with the ionic cores described by the Projector Augmented-Wave method (PAW),[38,39] which allows to use a low energy cut off equal to 500 eV for the plane-wave basis.

A (3 × 3 × 3) k-point grid was used in the Brillouin-zone sums, and the partial occupancies were set for each wave function using the tetrahedron method with Blöchl corrections.[40] The positions of all the atoms in the super cell as well as the cell parameters were relaxed in the potential energy determined by the full quantum mechanical electronic structure until the total energy differences between the loops decrease below 10^{-4} eV. The systems with unpaired electrons were calculated taking into account their spin state.

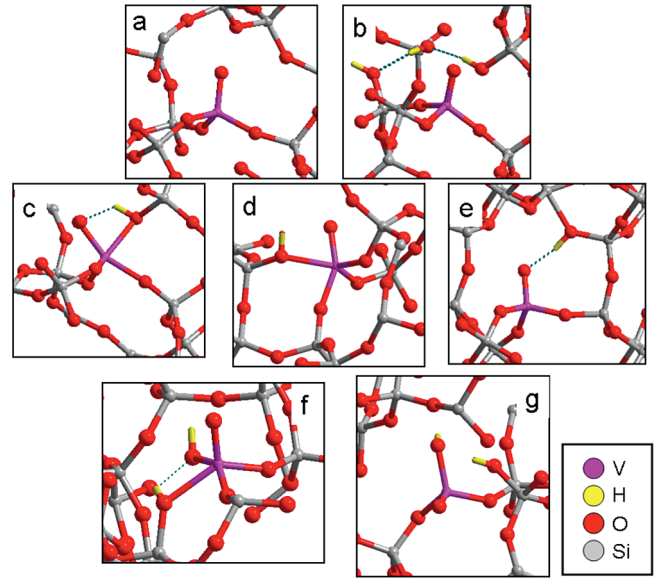

Figure 1. V models considered in this work.

To calculate the Hessian matrix, finite differences were used, that is, each ion is displaced in the direction of each Cartesian coordinate, and the Hessian matrix was determined from the forces. The frequency calculations were performed considering only the Gamma point.

The zeolite structure was modeled using a periodic three-dimensional sodalite structure, which has been shown to give reliable results as far as framework sites are concerned. We refer to our former work[12] for more details. In this study, the set of V-framework sites is extended to sites containing H-bond network (Figure 1), which was not considered earlier.[12]

3. Results and Discussion

3.1. Characterization of Silicon Environment. ***3.1.1. FTIR.*** As reported earlier,[6] the parent BEA zeolite exhibits an IR spectrum (results not shown) with bands due to hydroxyls: AlO−H at 3780 and 3662 cm^{-1} and Si−O(H)−Al at 3609 cm^{-1}. As expected, these three bands are eliminated upon dealumination, concomitantly, new IR bands develop at 3736 cm^{-1}, due to isolated SiO−H groups; a shoulder at 3710 cm^{-1} due to terminal SiO-H groups and a broad band at 3520 cm^{-1} attributed to H-bonded SiO-H groups.[6] The presence of a large amount of SiO−H groups in SiBEA was confirmed by the presence of an intense band near 960 cm^{-1} assigned to the stretching of Si−O bonds.[6]

3.1.2. Raman. The Raman spectrum of SiBEA zeolite exhibits band at 1063 cm^{-1} (weak) related to transverse-optical asymmetric stretch (Figure 2A).[41,42] It disappears upon vanadium incorporation into SiBEA zeolite, because of its overlap with the V−O−Si asymmetric stretching Raman mode (1070−1063 cm^{-1}).[46] A weak band at 967 cm^{-1} in SiBEA corresponds to connectivity defects (Si−O−Si) and/or Si−OH stretching mode of surface hydroxyls (Figure 2A).[41−43] It confirms the removal of aluminum from the zeolite framework.

Raman spectra of SiBEA zeolite and V_xSiBEA zeolites exhibit bands corresponding to the silicalites framework breathing modes (550−250 cm^{-1}), silica network symmetric stretch

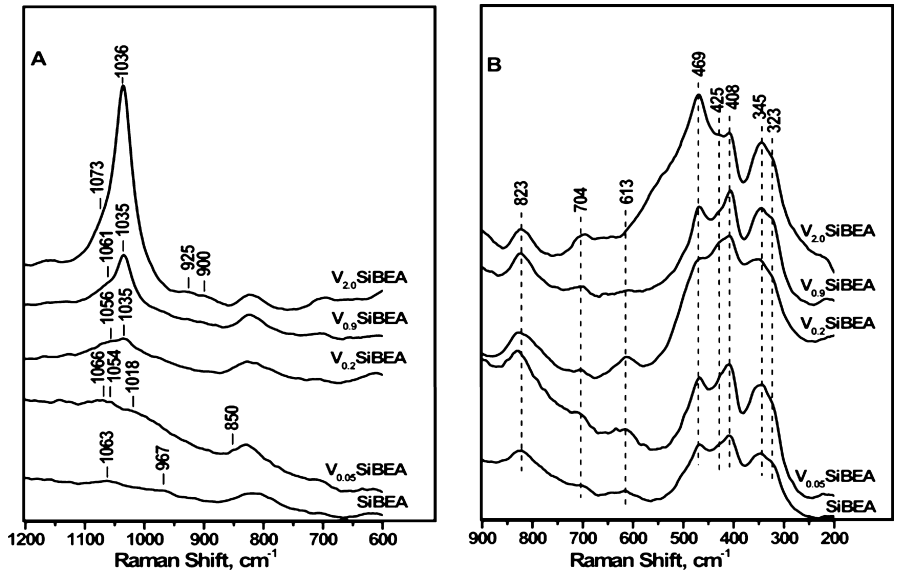

Figure 2. Raman spectra of SiBEA, $V_{0.05}$SiBEA, $V_{0.2}$SiBEA, $V_{0.9}$SiBEA, and $V_{2.0}$SiBEA recorded under dehydrated conditions at 773 K after 2 h calcination in air at 773 K. Panel A is for the 1200−600 cm^{-1} range and panel B is for the 900−200 cm^{-1} range.

(823 cm^{-1}) and Si−O bonds (704 cm^{-1}) (Figure 2B).[43−45] O-localized modes of the TO_4-rings building up the structure of the framework generate Raman breathing modes,[43−45] which are sensitive to the type and distribution of the closed contours of T-O bonds. The Raman band at 464 cm^{-1} is assigned to four-membered rings, those at 425 and 408 cm^{-1} to six-membered rings, and those at 355 and 323 cm^{-1} to five-membered rings. The periodic building units (intralayer ring) of zeolite BEA exhibit Raman bands at 464, 408, and 323 cm^{-1}. The bands at 425 and 355 cm^{-1} are typical of the interlayer connectivity modes (interlayer ring).[43−45] The presence of silicalites framework breathing modes (550−250 cm^{-1}) after vanadium incorporation confirms the stability of BEA zeolite after dealumination and vanadium incorporation.

3.2. Characterization of Vanadium Environment. ***3.2.1. DR UV−vis.*** DR UV−vis spectroscopy allows one to detect V(IV) and V(V) species as well as to distinguish tetrahedral from octahedral vanadium species. The UV−vis spectra of $V_{0.05}$SiBEA, $V_{0.2}$SiBE, $V_{0.9}$SiBEA, and $V_{2.0}$SiBEA (Figure 3) exhibit two bands near 265 and 340 nm attributed to $\pi(t_2)\rightarrow$d(e) and $\pi(t_1)\rightarrow$d(e) oxygen-to-tetrahedral V(V) charge transfer transitions, involving oxygen in bridging (V−O−Si) and terminal (V═O) positions, respectively, in line with earlier results.[13] The intensities of both bands increase with vanadium loading (Figure 3). The absence of (d−d) transitions in the 600−800 nm range indicates that there is not a significant presence of V(IV) species.

3.2.2. Raman. Dehydrated V_xSiBEA samples exhibit Raman bands related to silicalite framework and vibrational modes related to dispersed VO_x species (Figure 2A,B). Silicalite framework Raman features dominate the spectrum of the catalyst with the lowest vanadium content (0.05 wt %) (Figure 2A). The weak Raman band at 1067 cm^{-1} is assigned to antisymmetric V−O−Si mode and/or to zeolite framework Raman mode.[46] Two bands at 1054 and 1018 cm^{-1} are assigned to V═O modes in two kinds of framework V(V). The band at 1054 cm^{-1} corresponds probably to V═O mode in nonhydroxylated tetrahedral vanadium species (SiO_3)V═O related to a model a in Figure 1. A weak band at 1018 cm^{-1} results from a partially hydroxylated pyramidal $(SiO)_2$(HO)V═O structure with one OH group in the vanadium coordination sphere (Figure 2A). The existence of a partially hydroxylated pyramidal structure with

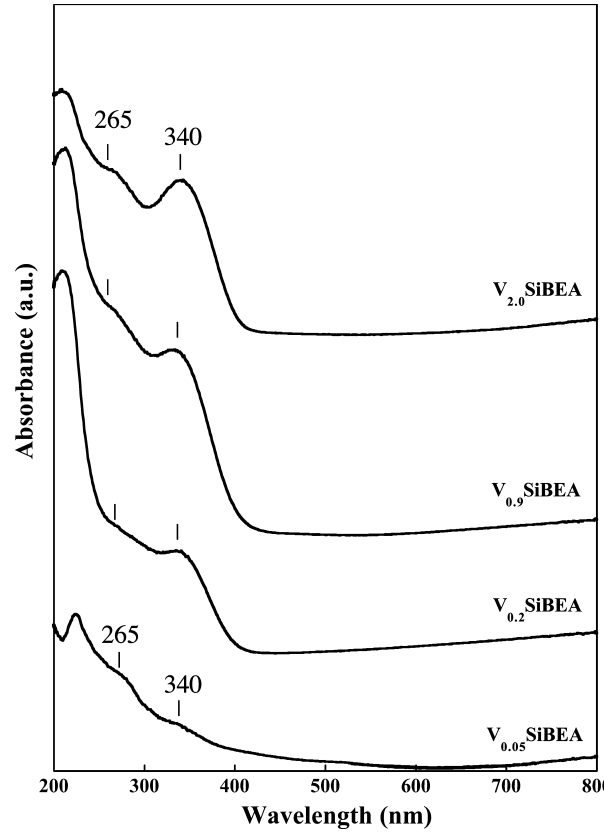

Figure 3. DR UV−vis spectra recorded at ambient atmosphere of $V_{0.05}$SiBEA, $V_{0.2}$SiBEA, $V_{0.9}$SiBEA, and $V_{2.0}$SiBEA as prepared.

one hydroxyl group hydrogen-bonded to the bridging oxygen atom in the V−O−Si (band at 1032 cm^{-1}) was identified for highly dehydrated silica surface.[46] Such work reports a red shift for the hydroxylated site compared to the nonhydoxylated one. A weak band at 850 cm^{-1} appears to be related to symmetric V−O−Si modes. Such frequencies present a shift with respect to those described for silica support, which appears related to the zeolite nature of the support. DFT calculations of different silica-supported vanadia models reveal that the monomeric vanadium oxide species are sensitive to structure surrounding the vanadium species.[47]

TABLE 1: Calculated Vibration Frequencies for the Different Vanadium Model Sites Considered (a−g, See Figure 1) in This Work[a]

experiment		calculated						
low V content (0.05 wt %)	high v content (0.2−2 wt %)	**a**	**b**	**c**	**d**	**e**	**f**	**g**
1067	1073		1071				1059	1059 (V═O)
1053	1035	1049 (V═O)	1051	1048 (V═O)		1044	1040 (V═O)	
		1033	1042		1029	1038	1031	1033
1018			1023 (V═O)		1018			
998			1017				997	
				978		975 (V═O)		977
		920	937		931 (V═O)		921	
	900	901			910	910		
						883		885
				870	864			
850								

[a] The frequencies are in cm^{-1} and corrected with a scaling factor of 0.979.[12]

Dehydrated V_xSiBEA samples with higher vanadium content (>0.2 wt %) show a Raman band at 1035 cm^{-1} (Figure 2A), attributed to the stretching mode of terminal V═O bond of the nonhydroxylated $(SiO)_3V═O$ site. The concentration of nonhydroxylated species increases with vanadium content. The Raman shoulder at 1060−1070 cm^{-1} is assigned to the antisymmetric V−O−Si stretching mode and the band at 900 cm^{-1} to the symmetric V−O−Si stretching mode.[23,47,46] The V−O−Si vibrational modes present a significantly lower intensity than that of the vanadyl modes and are much broader.

Raman data of dehydrated V_xSiBEA catalysts presented here are consistent with previous photoluminescence data.[7] For calcined V_xSiBEA (3 h at 773 K in flowing air) with very low V content (0.05 wt %), two fine structures were identified[7] with a vibrational energy of 1018 and 1054 cm^{-1} corresponding to the presence of the hydroxylated pyramidal structure $(SiO)_2(HO)V═O$ interacting with two nearby SiOH groups and of the nonhydroxylated pyramidal structure $(SiO)_3V═O$ not interacting with any SiOH group respectively. In contrast, for calcined V_xSiBEA with higher vanadium content (>0.2 wt %), one main fine structure was identified[7] with a vibrational energy of 1036 cm^{-1} corresponding to the presence of the nonhydroxylated pyramidal structure $(SiO)_3V═O$ interacting with one nearby SiOH group.

3.2.3. Computational Results. To shed some light on the assignment of spectroscopic data (IR, Raman, UV−vis, and so forth), quantum chemical calculations were performed. In an earlier attempt based on DFT calculations[12] on a set of vanadium environments, local variations such as the presence of H-bond interactions were not considered. It was concluded that the most stable V site had a tetrahedral pyramid-like $(SiO)_3V═O$ structure without V−OH groups. The metastable penta-coordinated $(SiO)_4VOH$ site exhibits IR bands at 3650 and 3620 cm^{-1}. However, these two bands could be due also to the presence of two distinct crystallographic sites and/or to V═O sites with or without V−OH groups in interaction with neighboring silanol groups.

Seven different models (from **a** to **g**) were built in order to assess the stability of the vanadyl site in the presence of H-bonds and V−OH groups (Figure 1). The following structures were considered:

model **a** is a nonhydroxylated $(SiO)_3V═O$ site without any defect in its direct vicinity (earlier called[12] model V5 and comparable, without Si^+ ions, to species labeled β as described earlier[7]);

model **b** is a nonhydroxylated $(SiO)_3V═O$ site with a H-bonded silanol in its vicinity, comparable to species labeled γ as described earlier;[7]

model **c** is a nonhydroxylated $(SiO)_3V═O$ site H-bonded to a silanol, forming site BV5,[12] or species labeled γ as reported earlier;[7]

model **d** has a similar configuration to model **c** but without H-bond between the vanadyl and the silanol, forming site BV5 as described earlier,[12] or species labeled γ as reported earlier;[7]

model **e** is a H-bonded nonhydroxylated $(SiO)_3V═O$ site with a nondirect bonded silanol or species labeled α as reported earlier;[7]

model **f** is a partially hydroxylated $(SiO)_2(HO)V═O$ site H bonded with a neighboring silanol forming site BTV5[12] or species labeled γ as described earlier;[7] and finally

model **g** is a non-H-bonded version of model **f** or species labeled α as reported earlier[7] corresponding to site VT5.[12]

On the basis of similar energy, the models can be subdivided into two isomeric groups, **a**, **c**, and **d** on one hand and **b**, **e**, **f**, and **g** on the other. In the first, model **a** is found to be by far the most stable site, which is in agreement with earlier work.[12] This model corresponds to an unperturbed tetrahedral $(SiO)_3V═O$ vanadyl site. The stability of the model decreases from **d** to **c**. Calculations show that H-bonded vanadyl groups are not energetically favored. Silanol groups prefer to form interacting silanol chains or nests, rather than to interact with a vanadyl group.

From the models of the second group (**b**, **e**, **f, g**) where there is a water molecule, **b** is the most stable model, which corresponds to a nonhydroxylated $(SiO)_3V═O$ site with one silanol in the neighborhood, followed by models **f**, **e**, and **g**. Model **e** with an H-bonded and nonhydroxylated $(SiO)_3V═O$ site is not very stable due to the distortions needed to form the H-bond. This structure could lead to a much more stable pentacoordinated $(SiO)_4VOH$ site, as shown earlier.[12]

The stability analysis of the different vanadium models evidence that a nonhydroxylated $(SiO)_3V═O$ site is likely to be the most frequent in vanadium-containing zeolites. Nevertheless, due to the particular synthesis method, that is, incorporation of vanadium ions into vacant T-atom sites associated with silanol groups, some silanol groups may not react with vanadium ions and might still be present in the neighborhood of vanadium site leading to the particular distortion of the vanadium site (model **b**, Figure 1). If this is the case, vibrational fingerprints should appear in the spectra, as will be shown below.

TABLE 2: Calculated Vibrational Frequencies for the Different Models Considered with Their Respective Vibrational Mode

	scaled freq	
a model		
3833	3753	SiOH
1072	1049	V═O
1055	1033	Si−O−V stretching in phase
940	920	Si−O−V stretching out of phase
920	901	Si−O−V stretching out of phase
b model		
3668	3591	SiOH
3758	3679	SiOH···H bond
3387	3316	SiOH···H bond
1094	1071	Si−O−V stretching in phase
1074	1051	Si−O−V stretching in phase
1064	1042	Si−O−V stretching in phase
1045	1023	V═O
1039	1017	Si−O−V stretching in phase
957	937	Si−O−V stretching out of phase
c model		
3325	3255	SiOH···O═V
1070	Coupled with framework 1048	SiOH···O═V stretching
999	978	Si−O−V stretching in phase
988	967	Si−O−V stretching in phase
889	870	Si−O−V stretching out of phase
852	834	Si−O−V stretching out of phase
d model		
3659	3582	SiOH···Hbond
1051	1029	Si−O−V stretching in phase
1040	1018	Si−O−V stretching in phase
951	931	V═O
930	910	Si−O−V stretching out of phase
883	864	Si−O−V stretching out of phase
e model		
3811	3731	SiOH
3804	3724	SiOH
3154	3088	SiOH···O═V
1066	1044	Si−O−V stretching in phase
1060	1038	Si−O−V stretching in phase
996	975	V═O
930	910	Si−O−V stretching out of phase
902	883	Si−O−V stretching out of phase
f model		
3830	3750	SiOH
3723	3645	VOH···H bonded
3401	3330	SiOHV
1082	1059	Si−O−V stretching in phase
1062	1040	V═O
1053	1031	Si−O−V stretching in phase
1018	997	Si−O−V stretching in phase
941	921	Si−O−V stretching out of phase
g model		
3835	3754	SiOH
3816	3736	SiOH
3753	3674	V−OH
1082	1059	V═O
1055	1033	Si−O−V stretching in phase
998	977	Si−O−V stretching in phase
904	885	Si−O−V stretching out of phase
901	882	Si−O−V stretching out of phase

The vibrational frequencies associated to the models have been calculated (Tables 1 and 2). One should note that significant couplings between bulk phonons and motions of the vanadium oxide site exist and that their vibrations cannot be separated from the silica framework.[47] Looking at the calculated frequencies, it is not straightforward to assign the experimental frequencies to a specific model. Models can be arranged into three groups (**a**, **b**), (**c**, **d**, **e**), and (**f**, **g**) as justified below.

Models **a** and **b** of the first group exhibit frequencies comparable with the experimental values for high-vanadium content 1073, 1035, and 900 cm^{-1}, assigned to in-phase Si−O−V, V═O, and out-of-phase Si−O−V modes, respectively. The first two bands overlap, depending on the presence/absence of hydroxyl groups in the neighborhood of the V═O group (model **a/b**, respectively). Thus, the Raman bands of dehydrated vanadium oxide species in high vanadium content correspond to tetrahedral V═O sites with or without silanol groups in their neighborhood. The theoretical frequencies are found to be 1049, 1033, 920, and 901 cm^{-1} for the unperturbed V═O site (model **a**), and 1071, 1051, 1023, 1017, and 937 cm^{-1} for the V═O site with silanols in its neighborhood. It is interesting to note that the frequencies at 1071 cm^{-1} correspond to the 1033 cm^{-1} band of the unperturbed model **a**. The deformation of the V site by neighboring silanol groups influences the Si−O−V. This result involves the choice of the model, and indeed, if this vibration mode is sensitive to local geometry distortions, the choice of the zeolite model would also influence the results, a point discussed earlier.[47]

At low vanadium content (0.05 wt %), the best fit between theory and experiment is obtained for models **f** and **g**. The Raman bands observed experimentally at 1053, 1018, 998, and 850 cm^{-1} can be assigned if the results of our models are associated with a V(OH)═O group (models **f** and **g**). Indeed, the theoretical frequencies (Tables 1 and 2) are the following: for model **f**, 1059, 1040, 1031, 997, and 921 cm^{-1}, and for model **g**, 1059, 1033, 977, and 885 cm^{-1}. As in the case of high vanadium content, the frequencies correspond to in-phase Si−O−V mode, V═O, in-phase Si−O−V mode, and out-of-phase Si−O−V mode, respectively. Some overlap of bands can occur for the V═O group and in-phase Si−O−V mode and between the in-phase Si−O−V and out-of-phase Si−O−V modes. It should be noted that both models (**f** and **g**) are energetically not much favored, as discussed above. Since models **f** and **g** are energetically unfavored compared with models **a** and **b**, one may expect that the Raman bands of the hydroxylated vanadyl sites are too weak to be detected for zeolites with high V content and that the vibrational fingerprints of the more stable sites predominate in the Raman spectrum.

It is difficult to assign the frequencies of models **c**, **d**, and **e.** This conclusion is in line with the fact that these structures have H-bonded V═O sites, which are found to be energetically unfavored, and thus less probable to be found in the zeolite. This is due to a lower interaction between SiOH and V═O groups than between SiOH and another SiOH group.[48,49]

4. Conclusions

The combined use of DR-UV−vis and Raman spectroscopies allows one to evidence three types of tetrahedral V(V) with different structure in V_xSiBEA zeolite. For very low V content (0.05 wt %), the majority of V(V) ions exhibits a strongly distorted tetrahedral structure with a nonhydroxylated pyramidal $(SiO)_3V═O$ structure with V═O stretching at 1054 cm^{-1}(model **a**), whereas a minority adopts a distorted tetrahedral structure with hydroxylated pyramidal $(SiO)_2(HO)V═O$ structure with V═O stretching at 1018 cm^{-1} (model **f**). In contrast, for higher V content (0.2−2 wt %), the main distorted V(V) species possesses a nonhydroxylated pyramidal $(SiO)_3V═O$ structure with V═O stretching at 1033−1036 cm^{-1} (model **b**).

Periodic DFT calculations confirm the presence of three (**a**, **b**, **f**) different types of V site in V-containing zeolites. The

experimental Raman bands recorded in low and high vanadium-containing V_xSiBEA were obtained and assigned using seven vanadium models. The difficulty to assign the vibrations in V-containing silica materials is confirmed due to the overlap of different critical vibrational fingerprints (V═O, and Si−O−V modes). Moreover, it was found that H-bond formation of SiOH with a V═O group is energetically unfavored.

Acknowledgment. Part of this work was performed using the HPC resources from GENCI-[CCRT/CINES/IDRIS] (Grant 2010-[x2010082022]) and the CCRE of Université Pierre et Marie Curie Paris. COST ACTION D36 (Working Group D36-006-06) and the Spanish Ministry of Education and Science CTQ2008-02461/PPQ are acknowledged for financial support. A.E.L. acknowledges the Spanish Ministry of Education and Science for a "Juan de la Cierva" postdoctoral position. S.D. gratefully acknowledges the CNRS (France) for financing his research position.

References and Notes

(1) Matsuoka, M.; Anpo, M. J. *Photochem. Photobiol. C* **2003**, *3*, 225.
(2) Anpo, M.; Higashimoto, S. *Stud. Surf. Sci. Catal.* **2001**, *13*, 4857.
(3) (a) Anpo, M.; Che, M. *Adv. Catal.* **1999**, *44*, 119. (b) Anpo, M.; Dzwigaj, S.; Che, M. *Adv. Catal.* **2009**, *52*, 1.
(4) Anpo, M.; Zhang, S. G.; Higashimoto, S.; Matsuoka, M.; Yamashita, H.; Ichihashi, H.; Matsumura, Y.; Souma, Y. *J. Phys. Chem. B* **1999**, *103*, 9295.
(5) Dzwigaj, S.; Peltre, M. J.; Massiani, P.; Davidson, A.; Che, M.; Sen, T.; Sivasanker, S. *Chem. Commun.* **1998**, 87.
(6) Dzwigaj, S.; Massiani, P.; Davidson, A.; Che, M. *J. Mol. Catal. A: Chem.* **2000**, *155*, 169.
(7) Dzwigaj, S.; Matsuoka, M.; Anpo, M.; Che, M. *J. Phys. Chem. B* **2000**, *104*, 6012.
(8) Anpo, M.; Higashimoto, S.; Matsuoka, M.; Zhanpeisov, N.; Shioya, Y.; Dzwigaj, S.; Che, M. *Catal. Today* **2003**, *78*, 211.
(9) Dzwigaj, S.; El Malki, E. L. M.; Peltre, M. J.; Massiani, P.; Davidson, A.; Che, M. *Top. Catal.* **2000**, *11/12*, 379.
(10) Dzwigaj, S.; Matsuoka, M.; Anpo, M.; Che, M. *Stud. Surf. Sci. Catal.* **2001**, *135*, 2402.
(11) Dzwigaj, S.; Matsuoka, M.; Franck, R.; Anpo, M.; Che, M. *J. Phys. Chem. B* **1998**, *102*, 6309.
(12) Tielens, F.; Calatayud, M.; Dzwigaj, S.; Che, M. *Microporous Mesoporous Mater.* **2009**, *119*, 137.
(13) Centi, G.; Perathoner, S.; Trifiro, F.; Aboukais, A.; Aïssi, C. F.; Guelton, M. *J. Phys. Chem.* **1992**, *96*, 2617.
(14) Kornatowski, J.; Wichterlova, B.; Jirkovsky, J.; Loeffler, E.; Pilz, W. *J. Chem. Soc., Faraday Trans.* **1996**, *92*, 1067.
(15) Morey, M.; Davidson, A.; Eckert, H.; Stucky, G. *Chem. Mater.* **1996**, *8*, 486.
(16) Striegman, A. E.; Eckert, H.; Plett, G.; Kim, S. S.; Anderson, M.; Yavrouin, A. *Chem. Mater.* **1993**, *5*, 1591.
(17) Schraml-Marth, M.; Wokaun, A.; Pohl, M.; Krauss, H. L. *J. Chem. Soc., Faraday Trans.* **1991**, *87*, 2635.
(18) Luan, Z.; Xu, J.; He, H.; Klinowski, J.; Kevan, L. *J. Phys. Chem.* **1996**, *100*, 19595.
(19) Gaon, X. T.; Bare, S. R.; Weckhuysen, B. M.; Wachs, I. E. *J. Phys. Chem. B* **1998**, *102*, 10842.
(20) Khodakov, A.; Olthof, B.; Bell, A. T.; Iglesia, E. *J. Catal.* **1999**, *181*, 205.
(21) Dzwigaj, S.; Matsuoka, M.; Anpo, M.; Che, M. *Catal. Lett.* **2001**, *72*, 211.
(22) Sulikowski, B.; Olejniczak, Z.; Wloch, E.; Rakoczy, J.; Valenzuela, R. X.; Cortés Corberàn, V. *Appl. Catal., A* **2002**, *232*, 189.
(23) Islam, M. M.; Costa, D.; Calatayud, M.; Tielens, F. *J. Phys. Chem. C* **2009**, *113*, 10740.
(24) Dzwigaj, S. *Curr. Opin. Solid State Mater. Sci.* **2003**, *7*, 461.
(25) Bourgeat-Lami, E.; Fajula, F.; Anglerat, D.; des Courières, T. *Microporous Mater.* **1993**, *1*, 237.
(26) Madic, C.; Begun, G. M.; Hahn, R. L.; Launay, J. P.; Thiessen, W. E. *Inorg. Chem.* **1984**, *23*, 469.
(27) Baes, C. F.; Mesmer, R. E. In *The Hydrolysis of Cations*; Wiley: New York, 1976; p 210.
(28) Conte, V.; Di Furia, F.; Moro, S. *J. Mol. Catal.* **1994**, *94*, 323.
(29) Kresse, G.; Hafner, J. *Phys. Rev. B* **1994**, *49*, 14251.
(30) Kresse, G.; Furthmuller, J. *Comput. Mater. Sci.* **1996**, *6*, 15.
(31) Perdew, J. P.; Burke, K.; Ernzerhof, M. *Phys. Rev. Lett.* **1996**, *77*, 3865.
(32) Perdew, J. P.; Burke, K.; Ernzerhof, M. *Phys. Rev. Lett.* **1997**, *78*, 1396.
(33) Zhang, Y. K.; Yang, W. T. *Phys. Rev. Lett.* **1998**, *80*, 890.
(34) Gu, X.; Ji, M.; Wei, S. H.; Gong, X. G. *Phys. Rev. B* **2004**, *70*, 205401.
(35) Tielens, F.; Andrés, J.; Van Brussel, M.; Buess-Herman, C.; Geerlings, P. *J. Phys. Chem. B* **2005**, *109*, 7624.
(36) Visart de Bocarmé, T.; Chau, T.-D.; Tielens, F.; Andrés, J.; Gaspard, P.; Wang, L. R. C.; Kreuzer, H. J.; Kruse, N. *J. Chem. Phys.* **2006**, *125*, 54703.
(37) Tielens, F.; Andrés, J. *J. Phys. Chem. C* **2007**, *111*, 10342.
(38) Blöchl, P. E. *Phys. Rev. B* **1994**, *50*, 17953.
(39) Kresse, G.; Joubert, J. *Phys. Rev. B* **1999**, *59*, 1758.
(40) Blöchl, P. E.; Jepsen, O.; Andersen, O. K. *Phys. Rev. B* **1994**, *49*, 16223.
(41) Lee, E. L.; Wachs, I. E. *J. Phys. Chem. C* **2007**, *111*, 14410.
(42) Lee, E. L.; Wachs, I. E. *J. Phys. Chem. C* **2008**, *112*, 6287.
(43) Mihailova, B.; Valtchev, V.; Mintova, S.; Faust, A. C.; Petkov, N.; Bein, T. *Phys. Chem. Chem. Phys.* **2005**, *7*, 2756.
(44) Tosheva, L.; Mihailova, B.; Valtchev, V.; Sterte, J. *Microporous Mesoporous Mater.* **2001**, *48*, 31.
(45) Majano, G.; Mintova, S.; Ovsitser, O.; Mihailova, B.; Bein, T. *Microporous Mesoporous Mater.* **2005**, *80*, 227.
(46) Wu, Z.; Dai, Sh.; Overbury, S. H. *J. Phys. Chem. C* **2010**, *114*, 412.
(47) Döbler, J.; Pritzsche, M.; Sauer, J. *J. Phys. Chem. C* **2009**, *113*, 12454.
(48) Tielens, F. *J. Comput. Chem.* **2009**, *30*, 1946.
(49) Tielens, F. *J. Mol. Struct. (THEOCHEM)* **2009**, *903*, 23.

JP107589D